

White Aggregation and Restoration for Few-shot 3D Point Cloud Semantic Segmentation

Jiyeon Im*, SuBeen Lee*, Miso Lee, Jae-Pil Heo*
Sungkyunkwan University

{bbangs10110, leesb7426, dlalth557, jaepilheo}@skku.edu

Abstract

Few-Shot 3D Point Cloud Segmentation (FS-PCS) aims to predict per-point labels for an unlabeled point cloud, given only a few labeled examples. To extract discriminative representations from the limited support set, existing methods have constructed prototypes using conventional algorithms such as farthest point sampling. However, we point out that its initial randomness significantly affects FS-PCS performance and that the prototype generation process remains underexplored despite its prevalence. This motivates us to investigate an advanced prototype generation method based on attention mechanism. Despite its potential, we found that vanilla module suffers from the distributional gap between learnable prototypical tokens and support features. To overcome this, we propose White Aggregation and Restoration Module (WARM), which resolves the misalignment by sandwiching cross-attention between whitening and coloring transformations. Specifically, whitening aligns the support features to prototypical tokens before attention process, and subsequently coloring restores the original distribution to the attended tokens. This simple yet effective design enables robust attention, thereby generating representative prototypes by capturing the semantic relationships among support features. Our method achieves state-of-the-art performance with a significant margin on multiple FS-PCS benchmarks, demonstrating its effectiveness through extensive experiments.

1. Introduction

Understanding the semantics of 3D point clouds has become crucial as its applications have advanced [6, 31]. Although recent methods have achieved remarkable performance, they rely on large amounts of labeled data, which requires expensive labor [4, 9]. To alleviate this data reliance, Few-Shot 3D Point Cloud Segmentation (FS-PCS) was in-

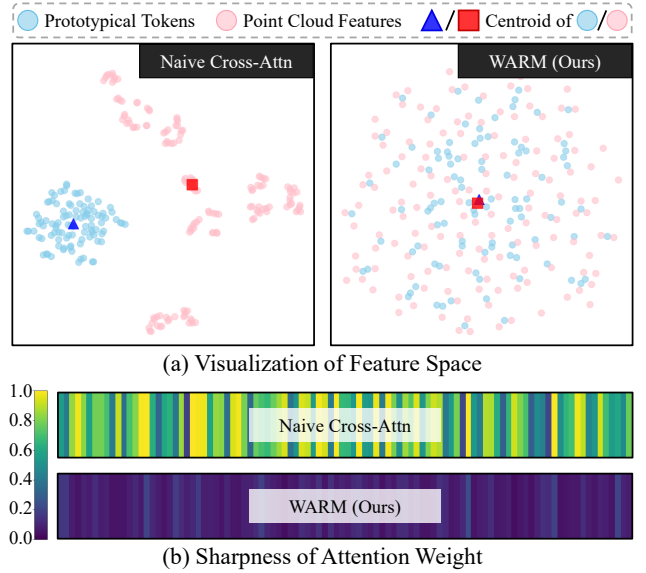


Figure 1. **(a)** Alignment between prototypical tokens and point cloud features depicted with t-SNE. In naïve cross-attention, queries (prototypical tokens) are often misaligned with keys (point cloud features), resulting in inaccurate matching that fails to capture relational structures between keys. In contrast, our method facilitates alignment between queries and keys, leading to more stable matching that reflects the semantic relationships among keys. **(b)** Sharpness of attention weight. Due to the misalignment between queries and keys, naïve cross-attention produces overly peaky attention weights. This constrains the representation of the naïve attention to a narrow spatial focus, almost point-level. On the other hand, our method shows relatively smooth weight distributions, which enable the attention to jointly attend to structurally and semantically related regions, thereby facilitating richer context aggregation.

roduced [36]. It aims to segment unlabeled point clouds, called a query set, using a small number of labeled point clouds, known as a support set.

To fully utilize the information from a few support set, previous studies have constructed prototypes [2, 36, 38]. It

* Equal contribution

* Corresponding author

Method	Best initialization			Worst initialization		
	S-0	S-1	Mean	S-0	S-1	Mean
COSeg	60.29	60.64	60.47	35.86	36.56	36.21
FPS + <i>min-dist</i>	59.48	53.10	56.29	45.04	39.52	42.28

Table 1. Performance comparison across seeds on the S3DIS dataset in the 1-way 1-shot scenario. ‘FPS + *min-dist*’ denotes a simple baseline method that assigns labels solely based on feature distances, after constructing prototypes using FPS. The best and worst performances are derived by selecting the highest and lowest results among 1,000 different initial seeds.

is widely adopted in other few-shot downstream tasks as their representation quality substantially affects the performance [12, 19, 22, 27, 34]. In FS-PCS, most existing methods have relied on conventional prototype generation strategies such as Farthest Point Sampling (FPS) [2, 3, 20, 24, 36].

Surprisingly, it causes severe performance instability as shown in Tab. 1. In particular, even the subsequent sophisticated module [2] fails to solve the task under the worst initialization. By contrast, a simple feature distance-based method outperforms it, highlighting the importance of prototype construction in FS-PCS. This motivates us to devise an advanced, consistent prototype generation module. One may consider the attention mechanism [28] as a promising candidate, given its demonstrated adaptability to prototype generation [12, 19, 22, 27, 34].

Nevertheless, we find that attention alone remains insufficient in case of FS-PCS. Ideally, the cross-attention module should be optimized such that the learnable prototypical tokens adaptively aggregate information from support features to form effective prototypes. However, this process fails due to a large distributional gap—not only between the prototypical tokens and the support point features, but also within the support features themselves, as illustrated in Fig. 1 (a). This misalignment prevents the prototypical tokens from capturing semantically meaningful relationships, and causes them to attend to only a few point, resulting in poor representation quality [11, 15, 18, 33]. As shown in Fig. 1 (b), most tokens assign over half of their total attention weight to a single support point, underscoring a lack of compositional understanding over the support set.

To this end, we propose White Aggregation and Restoration Module (WARM), which is the extended cross-attention module sandwiched between whitening and coloring transformations. Specifically, WARM first applies whitening [5], which is a standardization transform that removes correlations, to the support features to align with the prototypical tokens. By sharing the feature space, the tokens actively interact with the features, enabling adaptive semantic representations rather than local ones, as illustrated in Fig. 1 (b). Moreover, decorrelating feature channels leads to

smoother and more stable optimization [10, 14]. Thereafter, coloring—the inverse operation of whitening—restores the removed statistics to the resulting prototypes, preserving essential feature properties for comprehensive representation. Ultimately, WARM contributes to effective prototype generation by improving compatibility between learnable prototypes and support features, while also fostering stable optimization.

As a result, our proposed method achieves state-of-the-art performance on FS-PCS datasets [4, 9] with significant margins. We validate our method through extensive experiments, showing its effectiveness in addressing the aforementioned issues and improving performance via better feature alignment and channel decorrelation. The significance of our work lies in rethinking a simple architecture in light of task-specific challenges—an aspect often overlooked in recent FS-PCS literature—and introducing a complementary perspective for future research.

In summary, our contributions are as follows:

- We revisit the conventional algorithmic approaches in prototype generation for FS-PCS, and empirically demonstrate their limitations in terms of inconsistency.
- We propose WARM, an extended cross-attention module tailored to FS-PCS, which resolves the misalignment by incorporating whitening and coloring transformations into the attention process.
- We validate the effectiveness of WARM through extensive experiments, including significant performance gains and comprehensive ablation analyses.

2. Related Works

2.1. Few-Shot 3D Point Cloud Segmentation

Few-Shot 3D Point Cloud Segmentation (FS-PCS) aims to predict per-point labels for a query point cloud given a small set of labeled support samples. Following the prototypical paradigm [27], prior FS-PCS methods construct prototypes to represent the support-set information. Given the limited supervision, the expressiveness of these prototypes is crucial to performance. Most existing works adopt the multi-prototype pipeline introduced by [36], where seeds are selected via Farthest Point Sampling (FPS) in coordinate [2, 3] or feature space [20, 36], followed by clustering the surrounding features to form prototypes. Alternatively, some methods use a single prototype derived from masked average pooling [13, 38].

While these approaches are intuitive, they rely on hand-crafted rules, and most studies focus on adapting such fixed prototypes to the query rather than improving the prototype construction itself [20, 24]. In contrast, we explore a learnable alternative based on attention mechanisms to enhance the flexibility and expressiveness of prototype generation.

2.2. Attention-based Prototype Generation

In the image domain, it is common to construct prototypes using learnable prototypical tokens through cross-attention mechanisms, such as DETR [7] and Mask2Former [8]. In contrast, 3D domains typically adopt non-learnable, non-parametric tokens sampled directly from the input point cloud to summarize features via attention [21, 23, 26]. Although a few studies leverage parametric tokens in 3D [30, 32], they usually rely on auxiliary information such as camera coordinates or 2D image features. This tendency primarily arises from the inherent difficulty of aligning the point cloud distribution with parameter initializations [37].

Through our work, we inspect the underlying matter that creates the misalignment between point cloud features and prototypical tokens, and propose a novel approach that enables attention-based prototype generation in FS-PCS.

3. Preliminary

3.1. Problem Formulation

FS-PCS aims to segment unlabeled point clouds based on a small set of labeled points. Formally, in each N -way K -shot episode following the well-known meta-learning paradigm [29], it consists of K labeled point clouds for N classes, called the support set $S = \{(X_{n,k}^S, Y_{n,k}^S)\}_{k=1}^K \}_{n=1}^N$ and U unlabeled ones, named the query set $Q = \{(X_u^Q, Y_u^Q)\}_{u=1}^U$. Here, X and Y represent the point cloud and its corresponding mask, respectively. As a result, the goal of FS-PCS is to predict per-point semantic labels for each query point cloud in Q , leveraging the information in the support set S . Note that training and testing utilize mutually exclusive class sets, $\mathcal{C}_{\text{base}}$ and $\mathcal{C}_{\text{novel}}$, individually, *i.e.*, $\mathcal{C}_{\text{base}} \cap \mathcal{C}_{\text{novel}} = \emptyset$. In the below sections, we assume a 1-way 1-shot setting for better clarity.

3.2. Farthest Point Sampling (FPS)

Given a point cloud $X \in \mathbb{R}^{L \times 3}$, we extract the point-wise features $F \in \mathbb{R}^{L \times D}$, where L and D denote the number of points and the feature dimension, respectively. For simplicity, we assume that both the support and query sets contain L points. We divide the support set into two semantic classes, foreground (FG) and background (BG), based on the ground-truth mask Y^S . For each class $c \in \{\text{FG}, \text{BG}\}$, we obtain the class-specific features $F_c^S \in \mathbb{R}^{L_c \times D}$.

To effectively leverage the information within a few labeled samples, FS-PCS methods typically construct prototypes using the Farthest Point Sampling (FPS) algorithm [2, 3, 20, 36]. The FPS algorithm starts from a randomly selected point feature for each class $F_{c,l}^S$, which serves as the initial element $r_{c,1}$ of the subset. Then, it iteratively expands the subset $R_{c,t} = \{r_{c,1}, \dots, r_{c,t}\}$ at each

step $t = 1, \dots, T$, as follows:

$$r_{c,t+1} = \arg \max_{f_c^S \in F_c^S \setminus R_{c,t}} \left(\min_{r_c \in R_{c,t}} \|f_c^S - r_c\|_2 \right). \quad (1)$$

The resulting subset $R_{c,T}$ serves as a compact set of representative point features for each class.

4. Motivation

4.1. Attention-based Prototype Generation

Despite FPS’s wide adoption in FS-PCS, it suffers from intrinsic randomness. As detailed in Sec. 3.2, it initiates by randomly selecting a seed point from the input point cloud. Then, it iteratively chooses the farthest point from the previously selected point set. As a result, the output of FPS is highly dependent on the initial random choice, leading to substantial performance variance, as shown in Tab. 1.

In contrast to FS-PCS [2, 3, 20, 36] that relies on conventional FPS despite its inherent limitations, other few-shot downstream tasks [19, 22, 27] have developed prototype generation techniques, particularly leveraging cross-attention mechanisms. These attention-based strategies offer notable advantages over traditional FPS-based ones. First, they yield deterministic outputs, ensuring consistent and stable performance regardless of the random seed. Furthermore, they are fully differentiable, unlike the non-learnable nature of FPS. Therefore, they can be optimized for tasks via end-to-end training. These strengths motivate us to adopt attention-based prototype generation in FS-PCS.

Formally, cross-attention $\text{CA}(\cdot, \cdot)$ is formulated as:

$$\text{CA}(u_1, u_2) := A(u_1, u_2)W_v(u_2), \quad (2)$$

$$\text{where } A(u_1, u_2) = \text{softmax}(W_q(u_1)(W_k(u_2))^T), \quad (3)$$

and $W_q(\cdot)$, $W_k(\cdot)$, and $W_v(\cdot)$ are projection layers for the *query*, *key*, and *value*, respectively. This can be applied to our task to construct support prototypes, as follows:

$$\hat{P}_c = P_0 + \text{CA}(P_0, F_c), \quad (4)$$

where $P_0 \in \mathbb{R}^{M \times D}$ and $\hat{P}_c \in \mathbb{R}^{M \times D}$ are prototypical tokens and prototypes, respectively.

4.2. Attention Misalignment in FS-PCS

To construct representative prototypes using the cross-attention mechanism, it is crucial that the attention in Eq. 3 effectively captures the underlying semantic relationships among the support features. Otherwise, the whole process is prone to yield sub-optimal outputs, often relying heavily on skip connections [11, 18, 33]. Unfortunately, we discovered a severe misalignment between the prototypical tokens and point features, as illustrated in Fig. 1 (a). As a result, the tokens fail to capture semantic, attending instead to features

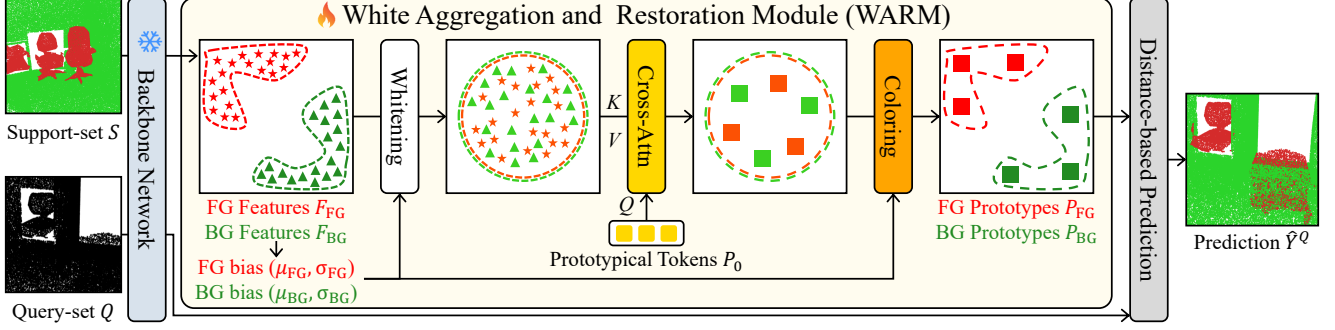


Figure 2. Overall pipeline in the 1-way 1-shot scenario. Initially, support and query features are extracted using a backbone network. Then, the support features are passed through the proposed WARM to generate prototypes. Within WARM, the support features are separated into foreground (FG) and background (BG) components, and each is individually whitened for temporary alignment with prototypical tokens. This whitening allows the prototypical tokens to aggregate each component based on semantic relationships via cross-attention. Subsequently, the original statistics are re-injected into the prototypes to restore their inherent characteristics. Finally, point-wise classification is performed on the query by assigning each point to its closest prototype.

Space	$\mathcal{D}_{\text{intra}}$	$\mathcal{D}_{\text{inter}}$	$\mathcal{D}_{\text{instance}}$
P_0	1.61	-	-
$W_q(P_0)$	1.62	-	-
F	134.17	185.26	95.06
$W_k(F)$	136.39	194.88	97.98

Table 2. Dispersion metrics on the S3DIS dataset under the 1-way 1-shot setting. P_0 , $W_q(P_0)$, F , and $W_k(F)$ denote learnable tokens, query embeddings, point features, and key embeddings in the attention mechanism, respectively. Each element of P_0 and $W_q(P_0)$ is treated as a prototype for computing $\mathcal{D}_{\text{intra}}$. The symbol ‘-’ indicates that the corresponding metric is not applicable.

that are proximal in the projection space, even when they are semantically irrelevant. In other words, this misalignment leads to prototypes that inadequately represent the semantic, remaining confined to point-level representations, as shown in Fig. 1 (b).

We analyze the problem in terms of the distribution in the embedding space of P_0 and F_{FG} to identify key factors of it. Note that we focus our analysis on the FG class only, since BG often contains a mixture of multiple semantic categories, which may introduce confounding factors. Concretely, the mean vector of support FG features $\mu_{\text{FG}} \in \mathbb{R}^D$ is defined as:

$$\mu_{\text{FG}} = \frac{1}{L_{\text{FG}}} \sum_{l=1}^{L_{\text{FG}}} F_{\text{FG},l}. \quad (5)$$

Then, we define two dispersion metrics, intra-class dispersion $\mathcal{D}_{\text{intra}}$ and inter-class dispersion $\mathcal{D}_{\text{inter}}$, as follows:

$$\mathcal{D}_{\text{intra}} = \|\mu_{\text{FG}} - \mu_{\text{FG}'}\|_2 \quad \text{where } \text{FG} = \text{FG}', \quad (6)$$

$$\mathcal{D}_{\text{inter}} = \|\mu_{\text{FG}} - \mu_{\text{FG}'}\|_2 \quad \text{where } \text{FG} \neq \text{FG}', \quad (7)$$

where $\mu_{\text{FG}'}$ denotes μ_{FG} from other episodes, while $\text{FG} = \text{FG}'$ means that the FG classes of two episodes are the same. Intuitively, $\mathcal{D}_{\text{intra}}$ measures the variation of instance centers within the same class, whereas $\mathcal{D}_{\text{inter}}$ quantifies the distance between different class centers. Tab. 2 shows that both $\mathcal{D}_{\text{inter}}$ and $\mathcal{D}_{\text{intra}}$ are high compared to the distribution of P_0 , indicating that all prototypes are highly separated from each other, regardless of the class. Such large distributional gaps across support sets not only hinder semantic correspondence during cross-attention, but also impede optimization [25].

Additionally, we define the instance-within dispersion $\mathcal{D}_{\text{instance}}$ as follows:

$$\mathcal{D}_{\text{instance}} = \frac{1}{L_{\text{FG}}} \sum_{l=1}^{L_{\text{FG}}} \|F_{\text{FG},l} - \mu_{\text{FG}}\|_2. \quad (8)$$

As shown in Tab. 2, $\mathcal{D}_{\text{instance}}$ computed from F is significantly higher than that from P_0 , indicating that even point features within each instance are widely scattered. This prevents relation-based aggregation within each instance, resulting in narrowly focused attention, as illustrated in Fig. 1. As a result, projecting disjoint support features into a more coherent and structured representation space becomes essential for effective aggregation.

5. Method

5.1. Overview

In this paper, we propose an advanced cross-attention module for FS-PCS: White Aggregation and Restoration Module (WARM). As illustrated in Fig. 2, WARM consists of three stages: whitening, cross-attention, and coloring. First, the support features are transformed into a whitened space by temporarily removing distributional statistics that hinder alignment between features and prototypical tokens.

This whitening facilitates the generation of compact prototypes through the cross-attention by emphasizing the semantic relationships of features in a shared space. However, the whitening process also removes unique characteristics inherent to individual support features. To preserve these important attributes, we restore the original distributional statistics to the attended prototypes via coloring. In summary, WARM enables alignment between the support set and the prototypical tokens, while retaining the original information of the support features.

5.2. White Aggregation and Restoration Module

As detailed in Sec. 4.2, the vanilla cross-attention is insufficient to aggregate point features based on their semantic relationships. This limitation arises from the extreme distributional statistics observed within each instance, which are not even consistently shared across instances of the same class, as shown in Tab. 2. Such statistics lead to a misalignment between the attention tokens and point features, ultimately hindering effective feature aggregation. To address this issue, we propose WARM, which improves alignment by temporarily removing the distributional statistics from the point features.

Specifically, for each class $c \in \{\text{FG}, \text{BG}\}$ in the support set, we compute the mean vector $\mu_c \in \mathbb{R}^D$ using Eq. 5, and the covariance matrix $\Sigma_c \in \mathbb{R}^{D \times D}$, as follows:

$$\Sigma_c = \frac{1}{L_c - 1} (F_c - \mathbf{1}_{L_c} \mu_c^\top)^\top (F_c - \mathbf{1}_{L_c} \mu_c^\top), \quad (9)$$

where $\mathbf{1}_{L_c} \in \mathbb{R}^{L_c \times 1}$ is a column vector of ones. Then, we apply ZCA whitening [5, 14] to F_c as follows:

$$Z_c = (F_c - \mu_c) \cdot (\Sigma_c)^{-\frac{1}{2}}, \quad (10)$$

where $Z_c \in \mathbb{R}^{L_c \times D}$ denotes the whitened features with zero mean and decorrelated channels, *i.e.*, $Z_c^\top \cdot Z_c = I$. By removing abnormal statistics, the whitened features reside in a standardized space, where attention tokens are better aligned with the point features. Leveraging the whitened support features Z_c , we generate prototypes $\tilde{P}_c \in \mathbb{R}^{M \times D}$, which replace those in Eq. 4, as follows:

$$\tilde{P}_c = P_0 + \text{CA}(P_0, Z_c). \quad (11)$$

This facilitates more stable and semantic-based aggregation, as the attention mechanism no longer needs to account for instance-specific distributional variations that lead to isolated pairwise matching.

Although the statistics discarded by whitening disrupt alignment during attention, prototypes representing support features should retain the statistics to preserve this complementary information and recover the original expressiveness of the features. To this end, we introduce a coloring

step after cross-attention. This can be simply implemented as the inverse of the ZCA whitening in Eq. 10, as follows:

$$P_c = \tilde{P}_c \cdot \Sigma_c^{\frac{1}{2}} + \mu_c, \quad (12)$$

where $P_c \in \mathbb{R}^{M \times D}$ denotes the final prototypes that incorporate complete information. As such, we obtain representative prototypes that are derived by considering semantic relationships within point clouds while restoring instance-specific distributional statistics.

5.3. Training Objective and Inference

We adopt a basic segmentation approach, in which each query point is assigned the class of its nearest prototype. The distance between l -th query point F_l^Q and the c -th class prototypes P_c is formulated as follows:

$$d_{c,l} = \min_{l'} \| F_l^Q - P_{c,l'} \|_2. \quad (13)$$

The prediction for the l -th query point is given as follows:

$$\hat{Y}_l^Q = \arg \min_c (d_{c,l}). \quad (14)$$

For supervision, we use a margin loss instead of the typical cross-entropy loss as our method is based on distance [35], as follows:

$$\mathcal{L}_{\text{margin}} = \sum_{l=1}^L \max(d_l^{\text{pos}} - d_l^{\text{neg}}, 0), \quad (15)$$

where d_l^{pos} and d_l^{neg} denote the distances to the prototype of the l -th query point's ground-truth class and to prototypes of the other classes, respectively. To further prevent the multi-prototypes from collapsing into trivial representations, we additionally apply a simplification loss [17], defined as:

$$\begin{aligned} \mathcal{L}_{\text{sim}} = \frac{1}{|c|} & \left(\frac{1}{L_c} \sum_{l=1}^{L_c} \min_m \| F_{c,l} - P_{c,m} \|_2 \right. \\ & + \frac{1}{M} \sum_{m=1}^M \min_l \| F_{c,l} - P_{c,m} \|_2 \\ & \left. + \max_m \min_l \| F_{c,l} - P_{c,m} \|_2 \right), \end{aligned} \quad (16)$$

where the loss is computed separately for foreground and background, encouraging the learnable tokens to resemble the original features while avoiding trivial solutions.

As a result, the overall training objective is defined as:

$$\mathcal{L} = \mathcal{L}_{\text{margin}} + \lambda \cdot \mathcal{L}_{\text{sim}}, \quad (17)$$

where λ is a coefficient hyperparameter, set to 0.5.

Method	1-way 1-shot			1-way 5-shot			2-way 1-shot			2-way 5-shot			Overall
	S-0	S-1	Mean	S-0	S-1	Mean	S-0	S-1	Mean	S-0	S-1	Mean	
AttMPTI [†]	40.72	40.20	40.46	53.07	47.88	50.48	35.33	33.61	34.47	42.21	37.07	39.64	41.26
COSeg	46.31	<u>48.10</u>	47.21	51.40	48.68	50.04	37.44	<u>36.45</u>	36.95	42.27	38.45	40.36	43.64
FPS + <i>min-dist.</i>	<u>51.35</u>	45.68	<u>48.52</u>	<u>68.43</u>	<u>61.51</u>	<u>64.97</u>	<u>44.48</u>	33.00	<u>38.74</u>	<u>58.22</u>	<u>45.52</u>	<u>51.87</u>	<u>51.03</u>
WARM	60.16	50.50	55.33	72.23	62.66	67.45	50.91	38.34	44.63	61.46	48.95	55.21	55.66

Table 3. Performance comparison on S3DIS dataset. The best and second-best results are **bolded** and underlined, respectively. † denotes reproduced performance without foreground leakage, obtained using the official code.

Method	1-way 1-shot			1-way 5-shot			2-way 1-shot			2-way 5-shot			Overall
	S-0	S-1	Mean	S-0	S-1	Mean	S-0	S-1	Mean	S-0	S-1	Mean	
AttMPTI [†]	33.55	30.52	32.04	45.81	40.63	43.22	26.08	23.66	24.87	34.86	29.41	32.14	33.07
COSeg	41.73	41.82	41.78	48.31	44.11	46.21	28.72	<u>28.83</u>	28.78	35.97	33.39	34.68	37.86
FPS + <i>min-dist.</i>	38.24	32.90	35.57	53.82	<u>46.15</u>	<u>49.99</u>	30.91	27.51	<u>29.21</u>	<u>44.04</u>	<u>39.57</u>	<u>41.81</u>	<u>39.15</u>
WARM	<u>40.57</u>	<u>38.95</u>	<u>39.76</u>	<u>53.40</u>	49.04	51.22	<u>30.27</u>	30.02	30.15	45.02	41.61	43.32	41.11

Table 4. Performance comparison on ScanNet dataset. The best and second-best results are **bolded** and underlined, respectively. † denotes reproduced performance without foreground leakage, obtained using the official code.

6. Experiments

6.1. Experimental Settings

6.1.1. Datasets.

We perform experiments on two benchmark datasets for FS-PCS: S3DIS [4] and ScanNet [9]. S3DIS comprises 271 indoor scenes with 12 semantic classes, and ScanNet contains 1,513 indoor scenes with annotations for 20 categories. For both datasets, the classes are split into two folds, S_0 and S_1 , for cross-validation, where they do not overlap with each other. Following prior work [36], each scene is divided into $1\text{m} \times 1\text{m}$ blocks. We adopt the same data preprocessing as in [2], where each block is voxelized into 0.02m grids, and up to 20,480 points are uniformly sampled per block to eliminate foreground leakage.

6.1.2. Implementation Details.

We use the encoder layers of Stratified Transformer [16] as the feature extractor, with pretrained weights from [2]. The feature extractor is kept frozen during all experiments. For prototype generation, we use a single WARM layer across datasets with 100 prototypical tokens for each foreground and background, totaling 200 tokens. Although we omit this distinction in the main text for simplicity, we maintain separate sets of 100 tokens for foreground and background in all experiments. In a multi-shot setting $K > 1$, we generate prototypes for each sample and average them across shots as in [27]. Evaluation is based on mean Intersection-over-Union (mIoU), and is performed on 1,000 episodes per class in the 1-way setting and 100 episodes per class combination for the 2-way setting to ensure stable results.

6.1.3. Training Environment.

We use the AdamW optimizer with a learning rate of 1×10^{-4} and a weight decay of 0.01. Training is conducted for 10 and 20 epochs for the N -way 1-shot and 5-shot settings, respectively, where each epoch consists of 400 episodes. The learning rate is decayed by a factor of 0.1 at 60% and 80% of the total number of epochs. All experiments are performed on a single RTX A6000 GPU.

6.2. Experimental Results

We compare WARM with existing baselines [2, 36] under 1-/2-way and 1-/5-shot settings. As described in Tab. 3, WARM achieves state-of-the-art performance on the S3DIS dataset across all scenarios, with a large margin. This superiority is consistently observed on the ScanNet dataset as well, as shown in Tab. 4.

Surprisingly, the effectiveness of WARM does not stem from incorporating a complex decoder, as in prior approaches [2, 36]. Rather, it comes from a principled design focused on prototype construction. Moreover, the competitive results of the simple FPS-based method, which merely assigns labels based on feature distance, further question the necessity of such complex decoders. These findings highlight the critical role of prototype quality in FS-PCS. Consequently, future work should increasingly focus on designing more expressive and robust prototypes, like other few-shot downstream tasks [12, 19, 34].

6.3. Ablation Study

All experiments are conducted using the 0-th fold under the 1-way 1-shot setting on the S3DIS [4].

	C	N	W	R	Dist(Q, K) ↓	S-0
(a)					288.81	47.29
(b)	✓				140.59	14.22
(c)		✓			13.30	14.18
(d)			✓		13.14	10.83
(e)	✓			✓	142.73	57.21
(f)		✓		✓	13.72	57.59
(g)			✓	✓	13.13	60.16

Table 5. Effectiveness of alignment. **C**, **N**, **W**, and **R** denote centering, normalization, whitening, and coloring. Centering refers to zero-centering the point features by subtracting their mean, while normalization means scaling the features to unit variance along each channel dimension. Dist(Q, K) indicates the distance between queries and keys under the cross-attention mechanism.

6.3.1. Component Ablation.

Tab. 5 shows a component-wise ablation study to verify the effectiveness of each alignment step. In (a), the naïve cross-attention suffers from severe misalignment between query and key features, as reflected in the large Dist(Q, K). To mitigate this, we propose a whitening-based alignment, while also considering alternative approaches such as centering and normalization. As shown in (b), centering, which shifts the centroid of features to zero, slightly alleviates the misalignment. However, it fails to resolve the high intra-instance dispersion, as discussed in Tab. 2. In contrast, normalization in (c) standardizes the features to unit variance along each channel dimension, further reducing the dispersion. Nonetheless, since it preserves the covariance structure, it remains sub-optimal compared to (d), where whitening enforces an isotropic distribution by removing the covariance. Although these alignment methods enable the cross-attention mechanism to capture semantic relationships within point features, they also eliminate essential distributional characteristics. As a result, the resulting prototypes cannot represent the inherent semantics of the original instance. To address this, coloring in (e–g) should be accompanied with the alignment process to restore the unique properties of the point features. Ultimately, the full model in (g), which combines whitening and coloring, achieves the best performance. This confirms the importance of not only aligning features for better attention but also restoring their original semantics for faithful prototype representation.

6.3.2. Semantic Attention by Whitening.

To verify that whitening enables prototypical tokens to aggregate point features based on their semantic relationships, we conduct both qualitative and quantitative analyses. First, we define two metrics: entropy, which measures the uniformity of each attention distribution and is normalized to the range $[0, 1]$; and diversity, which quantifies the distinct-

Method	Attention Entropy	Attention Diversity
Cross-Attention	0.2079	0.8824
WARM	0.8387	0.6442

Table 6. Quantitative comparison of attention maps. Entropy (normalized to the range $[0, 1]$) measures the uniformity of each attention distribution. Diversity is computed as the inverse of average similarity among the attention maps of the prototypical tokens, reflecting how distinctly they focus on different regions.

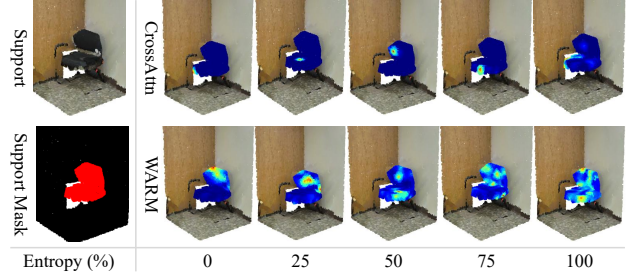


Figure 3. Qualitative comparison of attention maps. For a fair comparison, each attention map is selected according to its position within the entropy score distribution.

tiveness among prototypical tokens by computing the inverse of average similarity across their attention maps. As described in Tab. 6, the naïve cross-attention yields a low entropy score and a high diversity score. These scores imply that the prototypical tokens fail to capture the semantic structure of point features, instead focusing on features that are merely close in the projection space despite lacking semantic relevance. As a result, the attention collapses into point-level aggregation without meaningful semantic grouping. In contrast, our WARM with whitening achieves a relatively lower, yet sufficient, diversity score and a significantly higher entropy score. This suggests that each prototype attends more broadly and evenly to semantically related regions, resulting in richer and more coherent representations. Furthermore, the qualitative results in Fig. 3 support this observation. While the naïve attention focuses narrowly with limited spatial coverage, WARM highlights semantically coherent groupings of points. Note that these visualizations are selected based on percentile sampling of entropy scores, rather than cherry-picked examples.

6.3.3. Optimization Benefits of Whitening.

Beyond aligning queries and keys in the cross-attention, whitening provides auxiliary benefits for optimization. The original point features might exhibit correlations across channels, which may interfere with efficient learning by introducing redundancy [1]. By applying whitening, these correlations can be effectively eliminated. As illustrated in Fig. 4, WARM achieves faster convergence by maintaining higher gradient magnitudes throughout training. Despite the

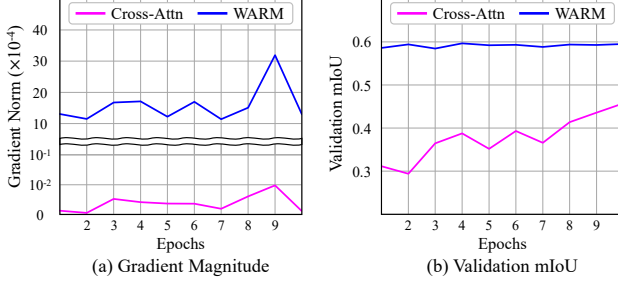


Figure 4. Training stability and acceleration by whitening.

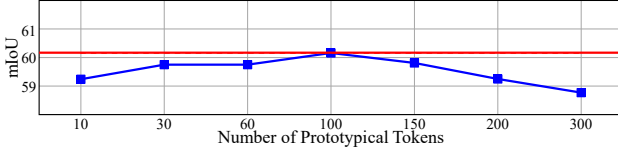


Figure 5. Ablation study of the number of prototypical tokens. The red line indicates the performance reported in the main results.

increased gradient flow, the training remains stable, suggesting that whitening enhances both optimization speed and robustness.

6.3.4. Number of Prototypical Tokens.

As illustrated in Fig. 5, WARM remains robust across a wide range of prototypical token counts, except when the number deviates significantly from the optimal range. These consistent trends indicate that our method is robust to the number of prototypical tokens.

7. Conclusion

In this paper, we investigated prototype generation for FS-PCS, addressing the limitations of conventional approaches in few-shot settings. We observed that even widely adopted mechanism struggles to bridge the distributional gap when trained with limited samples, motivating our design of an enhanced cross-attention module that incorporates whitening and coloring transformations. Through this design, we obtained representative prototypes by decoupling detrimental factors while preserving originality, thus achieving state-of-the-art performance across FS-PCS benchmarks with a significant margin. Pointing out the underexplored impact of prototype generation, we hope our work offers a complementary direction for FS-PCS.

References

- [1] Nasir Ahmad. Correlations are ruining your gradient descent. *arXiv preprint arXiv:2407.10780*, 2024. 7
- [2] Zhaochong An, Guolei Sun, Yun Liu, Fayao Liu, Zongwei Wu, Dan Wang, Luc Van Gool, and Serge Belongie. Re-thinking few-shot 3d point cloud semantic segmentation. *Proceedings of the IEEE/CVF conference on computer vision and pattern recognition*, pages 3996–4006, 2024. 1, 2, 3, 6
- [3] Zhaochong An, Guolei Sun, Yun Liu, Runjia Li, Min Wu, Ming-Ming Cheng, Ender Konukoglu, and Serge Belongie. Multimodality helps few-shot 3d point cloud semantic segmentation. In *ICLR*, 2025. 2, 3
- [4] Iro Armeni, Ozan Sener, Amir R Zamir, Helen Jiang, Ioannis Brilakis, Martin Fischer, and Silvio Savarese. 3d semantic parsing of large-scale indoor spaces. In *Proceedings of the IEEE conference on computer vision and pattern recognition*, pages 1534–1543, 2016. 1, 2, 6
- [5] Anthony J Bell and Terrence J Sejnowski. The “independent components” of natural scenes are edge filters. *Vision research*, 37(23):3327–3338, 1997. 2, 5
- [6] Thodoris Betsas, Andreas Georgopoulos, Anastasios Doulamis, and Pierre Grussenmeyer. Deep learning on 3d semantic segmentation: A detailed review. *Remote Sensing*, 17(2):298, 2025. 1
- [7] Nicolas Carion, Francisco Massa, Gabriel Synnaeve, Nicolas Usunier, Alexander Kirillov, and Sergey Zagoruyko. End-to-end object detection with transformers. In *European conference on computer vision*, pages 213–229. Springer, 2020. 3
- [8] Bowen Cheng, Ishan Misra, Alexander G Schwing, Alexander Kirillov, and Rohit Girdhar. Masked-attention mask transformer for universal image segmentation. In *Proceedings of the IEEE/CVF conference on computer vision and pattern recognition*, pages 1290–1299, 2022. 3
- [9] Angela Dai, Angel X Chang, Manolis Savva, Maciej Halber, Thomas Funkhouser, and Matthias Nießner. Scannet: Richly-annotated 3d reconstructions of indoor scenes. In *Proceedings of the IEEE conference on computer vision and pattern recognition*, pages 5828–5839, 2017. 1, 2, 6
- [10] Hadi Daneshmand, Jonas Kohler, Francis Bach, Thomas Hofmann, and Aurelien Lucchi. Batch normalization provably avoids ranks collapse for randomly initialised deep networks. *Advances in Neural Information Processing Systems*, 33:18387–18398, 2020. 2
- [11] Yihe Dong, Jean-Baptiste Cordonnier, and Andreas Loukas. Attention is not all you need: Pure attention loses rank doubly exponentially with depth. In *International conference on machine learning*, pages 2793–2803. PMLR, 2021. 2, 3
- [12] Qi Fan, Wenjie Pei, Yu-Wing Tai, and Chi-Keung Tang. Self-support few-shot semantic segmentation. In *European conference on computer vision*, pages 701–719. Springer, 2022. 2, 6
- [13] Shuting He, Xudong Jiang, Wei Jiang, and Henghui Ding. Prototype adaption and projection for few- and zero-shot 3d point cloud semantic segmentation. *IEEE Transactions on Image Processing*, 2023. 2
- [14] Lei Huang, Dawei Yang, Bo Lang, and Jia Deng. Decorrelated batch normalization. In *Proceedings of the IEEE Conference on Computer Vision and Pattern Recognition*, pages 791–800, 2018. 2, 5
- [15] Olga Kovaleva, Alexey Romanov, Anna Rogers, and Anna Rumshisky. Revealing the dark secrets of bert. *arXiv preprint arXiv:1908.08593*, 2019. 2

- [16] Xin Lai, Jianhui Liu, Li Jiang, Liwei Wang, Hengshuang Zhao, Shu Liu, Xiaojuan Qi, and Jiaya Jia. Stratified transformer for 3d point cloud segmentation. In *Proceedings of the IEEE/CVF conference on computer vision and pattern recognition*, pages 8500–8509, 2022. 6
- [17] Itai Lang, Asaf Manor, and Shai Avidan. Samplenet: Differentiable point cloud sampling. In *Proceedings of the IEEE/CVF conference on computer vision and pattern recognition*, pages 7578–7588, 2020. 5
- [18] Miso Lee, Jihwan Kim, and Jae-Pil Heo. Activating self-attention for multi-scene absolute pose regression. *Advances in Neural Information Processing Systems*, 37:38508–38529, 2024. 2, 3
- [19] SuBeen Lee, WonJun Moon, Hyun Seok Seong, and Jae-Pil Heo. Temporal alignment-free video matching for few-shot action recognition. In *Proceedings of the Computer Vision and Pattern Recognition Conference*, pages 5412–5421, 2025. 2, 3, 6
- [20] Zhaoyang Li, Yuan Wang, Wangkai Li, Rui Sun, and Tianzhu Zhang. Localization and expansion: A decoupled framework for point cloud few-shot semantic segmentation. In *European Conference on Computer Vision*, pages 18–34. Springer, 2024. 2, 3
- [21] Haotian Liu, Mu Cai, and Yong Jae Lee. Masked discrimination for self-supervised learning on point clouds. In *European Conference on Computer Vision*, pages 657–675. Springer, 2022. 3
- [22] Yongfei Liu, Xiangyi Zhang, Songyang Zhang, and Xuming He. Part-aware prototype network for few-shot semantic segmentation. In *European conference on computer vision*, pages 142–158. Springer, 2020. 2, 3
- [23] Ishan Misra, Rohit Girdhar, and Armand Joulin. An end-to-end transformer model for 3d object detection. In *Proceedings of the IEEE/CVF international conference on computer vision*, pages 2906–2917, 2021. 3
- [24] Zhenhua Ning, Zhuotao Tian, Guangming Lu, and Wenjie Pei. Boosting few-shot 3d point cloud segmentation via query-guided enhancement. In *Proceedings of the 31st ACM international conference on multimedia*, pages 1895–1904, 2023. 2
- [25] Shibani Santurkar, Dimitris Tsipras, Andrew Ilyas, and Aleksander Madry. How does batch normalization help optimization? *Advances in neural information processing systems*, 31, 2018. 4
- [26] Jonas Schult, Francis Engelmann, Alexander Hermans, Or Litany, Siyu Tang, and Bastian Leibe. Mask3d: Mask transformer for 3d semantic instance segmentation. *arXiv preprint arXiv:2210.03105*, 2022. 3
- [27] Jake Snell, Kevin Swersky, and Richard Zemel. Prototypical networks for few-shot learning. *Advances in neural information processing systems*, 30, 2017. 2, 3, 6
- [28] Ashish Vaswani, Noam Shazeer, Niki Parmar, Jakob Uszkoreit, Llion Jones, Aidan N Gomez, Łukasz Kaiser, and Illia Polosukhin. Attention is all you need. *Advances in neural information processing systems*, 30, 2017. 2
- [29] Oriol Vinyals, Charles Blundell, Timothy Lillicrap, Daan Wierstra, et al. Matching networks for one shot learning. *Advances in neural information processing systems*, 29, 2016. 3
- [30] Yue Wang, Vitor Campagnolo Guizilini, Tianyuan Zhang, Yilun Wang, Hang Zhao, and Justin Solomon. Detr3d: 3d object detection from multi-view images via 3d-to-2d queries. In *Conference on robot learning*, pages 180–191. PMLR, 2022. 3
- [31] Aoran Xiao, Jiaxing Huang, Dayan Guan, Xiaoqin Zhang, Shijian Lu, and Ling Shao. Unsupervised point cloud representation learning with deep neural networks: A survey. *IEEE Transactions on Pattern Analysis and Machine Intelligence*, 45(9):11321–11339, 2023. 1
- [32] Yiming Xie, Huaizu Jiang, Georgia Gkioxari, and Julian Straub. Pixel-aligned recurrent queries for multi-view 3d object detection. In *Proceedings of the IEEE/CVF International Conference on Computer Vision*, pages 18370–18380, 2023. 3
- [33] Shuangfei Zhai, Tatiana Likhomanenko, Etai Littwin, Dan Busbridge, Jason Ramapuram, Yizhe Zhang, Jiatao Gu, and Joshua M Susskind. Stabilizing transformer training by preventing attention entropy collapse. In *International Conference on Machine Learning*, pages 40770–40803. PMLR, 2023. 2, 3
- [34] Jian-Wei Zhang, Yifan Sun, Yi Yang, and Wei Chen. Feature-proxy transformer for few-shot segmentation. *Advances in neural information processing systems*, 35:6575–6588, 2022. 2, 6
- [35] Qin Zhang, Linghan Xu, Qingming Tang, Jun Fang, Ying Nian Wu, Joe Tighe, and Yifan Xing. Threshold-consistent margin loss for open-world deep metric learning. *arXiv preprint arXiv:2307.04047*, 2023. 5
- [36] Na Zhao, Tat-Seng Chua, and Gim Hee Lee. Few-shot 3d point cloud semantic segmentation. In *Proceedings of the IEEE/CVF conference on computer vision and pattern recognition*, pages 8873–8882, 2021. 1, 2, 3, 6
- [37] Xin Zhou, Dingkan Liang, Wei Xu, Xingkui Zhu, Yihan Xu, Zhikang Zou, and Xiang Bai. Dynamic adapter meets prompt tuning: Parameter-efficient transfer learning for point cloud analysis. In *Proceedings of the IEEE/CVF Conference on Computer Vision and Pattern Recognition*, pages 14707–14717, 2024. 3
- [38] Xiangyang Zhu, Renrui Zhang, Bowei He, Ziyu Guo, Jiaming Liu, Han Xiao, Chaoyou Fu, Hao Dong, and Peng Gao. No time to train: Empowering non-parametric networks for few-shot 3d scene segmentation. In *Proceedings of the IEEE/CVF conference on computer vision and pattern recognition*, pages 3838–3847, 2024. 1, 2